Epitaxial growth, structure, and intermixing at the $LaAlO_3/SrTiO_3$ interface as the film stoichiometry is varied

L. Qiao,[1] T. C. Droubay,[1] T. Varga,[2] M. E. Bowden,[2] V. Shutthanandan,[2] Z. Zhu,[2] T. C. Kaspar,[1] and S. A. Chambers[1,*]

[1]*Fundamental and Computational Science Directorate, Pacific Northwest National Laboratory, Richland, Washington 99352, USA*

[2]*Environmental and Molecular Sciences Laboratory, Pacific Northwest National Laboratory, Richland, Washington 99352, USA*

(Received 5 August 2010; revised manuscript received 10 December 2010; published 11 February 2011)

$LaAlO_3$ epitaxial films with La:Al cation ratios ranging from 0.9 to 1.2 were grown on TiO_2-terminated $SrTiO_3$ (001) substrates by off-axis pulsed laser deposition. Although all films are epitaxial, rocking curve measurements show that the crystallographic quality degrades with increasing La:Al ratio. Films with La:Al ratios of 0.9, 1.0, and 1.1 were coherently strained to the substrate. However, the out-of-plane lattice parameter increases over this range, revealing a decrease in film tetragonality. Although all film surfaces exhibit hydroxylation, the extent of hydroxylation is greater for the La-rich films. Rutherford backscattering spectrometry reveals that La from the film diffuses deeply into the $SrTiO_3$ substrate and secondary-ion-mass spectroscopy shows unambiguous Sr outdiffusion into the films.

DOI: 10.1103/PhysRevB.83.085408 PACS number(s): 05.70.Np, 61.50.Nw, 82.80.Yc, 68.49.Sf

I. INTRODUCTION

Perovskite oxides exhibit a wide range of electronic and magnetic properties spanning from superconductivity to insulating behavior, antiferromagnetism to ferromagnetism, paraelectricity to ferroelectricity, and possible multiferroic behavior.[1] The ability to control atomic structure and composition in complex oxides is emerging as one of the major challenges and opportunities for exploring and understanding functional properties in this broad class of materials. Perovskites, for which the chemical formula is ABO_3, consist of alternating layers of AO and BO_2 along the [001] direction. A range of cations can in principle be inserted into the A- and B-site sublattices to yield a wealth of compositions and structural distortions. As a result, epitaxial heterointerfaces based on these materials may exhibit unexpected properties not seen in analogous bulk materials.[2]

A particularly interesting example of this phenomenon is the observation of electronic conductivity at the interface of the two band insulators $LaAlO_3$ (LAO) and $SrTiO_3$ (STO).[3–6] Several candidate mechanisms have been proposed to account for this conductivity. The most prevalent is an electronic reconstruction to alleviate the polar discontinuity at the polar-nonpolar interface.[7,8] Others include oxygen vacancy formation in the substrate,[9,10] unintentional doping of the substrate by elements from the film,[11–13] and lattice distortions.[14] However, the actual mechanism of conductivity has not been unambiguously determined. Moreover, more than one mechanism may be operative depending on the exact state of the interface. For instance, if the interface intermixes in such a way that more La (a donor in STO) than Al (an acceptor in STO) indiffuses, the underlying STO may be net n type. If, however, equal amounts of La and Al indiffuse, there may be complete compensation of electrons and holes, and the doping effect will not result in conductivity. In this case, conductivity could result from an electronic reconstruction. In any event, knowledge of the film composition and atom distributions near the interface is essential for formulating realistic electronic structure models.

Pulsed laser deposition (PLD) is the most commonly used growth method for preparation of the LAO/STO interface. It is generally assumed that PLD results in stoichiometric transfer of LAO from the target to the film, provided the ablation threshold has been exceeded. However, a compositional analysis is done only infrequently. There are a few published studies that address deviations from stoichiometry in PLD-grown perovskites. Ohnishi *et al.*[15–17] have shown that the common practice of increasing the laser energy density above some material-specific threshold value to obtain stoichiometric films does not work for low-carrier-density materials such as STO. These authors have found that by increasing the laser energy density from 0.21 to 0.3 and 1.91 J cm^{-2}, the STO film composition transitioned from Sr rich to stoichiometric to Ti rich, and that these changes induced dramatic modifications in the electrical transport properties. This study also revealed that deviations in the lattice parameter, which are often ascribed to oxygen vacancy creation, may be the result of cation nonstoichiometry, as has been seen in STO grown by molecular beam epitaxy (MBE).[18] Likewise, Fisher *et al.*[19] and Fuchs *et al.*[20] demonstrated that the Sr/Ti cation ratio has a significant influence on surface reconstruction, long-range crystalline structure, and defect formation in STO grown by MBE and reactive sputtering, respectively. Jang *et al.*[21] recently demonstrated that small deviations from stoichiometry can induce non-negligible ferroelectricity in strain-free STO, which is typically an incipient ferroelectric and thought to exhibit ferroelectricity only when in a state of biaxial strain, or electric field or cation doping. Other papers focus on the effects of nonstoichiometry in the tetragonal perovskite $BaTiO_3$,[22,23] the layered perovskite $SrBi_2Ta_2O_9$,[24] trigonal $LiNbO_3$,[25] and spinel $LiMn_2O_4$.[26] However, there is little in the literature on the stoichiometry of PLD-growth LAO.

Another issue that has been given relatively little attention in the extensive LAO/STO literature is that of interfacial intermixing. It is generally assumed that the interface is essentially abrupt.[27] That is, cation exchange, if it is considered at all, is thought to be limited to within the first few atomic layers from the interface, with the extent of intermixing falling off sharply with distance from the interface. Limited intermixing has been observed or inferred using high-angle annular dark-field transmission-electron microscopy (HAADF-TEM),[7,28]

surface x-ray diffraction,[11] and medium-energy ion scattering (MEIS).[12] However, theoretical calculations on LAO/STO typically ignore intermixing and model the interface as being perfectly abrupt.[29–32] In contrast, we have recently published calculations that show that intermixing leads to significantly enhanced thermodynamic stability of the interface relative to the abrupt configuration, and that intermixing is essential in order to accurately predict band bending and the valence-band offset.[33]

Because interdiffusion at an interface is, at least in part, a kinetically controlled process, the actual structure and composition may vary significantly in samples grown in different laboratories, depending on the growth parameters and post-growth treatment. Moreover, the interface composition may vary from location to location within the same sample depending on the presence of defects in the substrate and defects that form at the interface as a result of lattice mismatch. Therefore, careful materials characterization of the interface is required. Here, we show that the composition of epitaxial LAO films grown by PLD varies significantly with the position of the substrate relative to the laser plume. Additionally, we show that cation nonstoichiometry influences crystalline quality, structure, and surface properties of LAO films. Rutherford backscattering and secondary-ion-mass spectrometries reveal La diffusion into the substrate and Sr diffusion into the film for both stoichiometric and nonstoichiometric LAO films.

II. EXPERIMENTAL

Epitaxial LAO films were grown on STO(001) by off-axis PLD. Substrates were etched in buffered HF, rinsed, and annealed in flowing O_2 (1 atm) at 1000 °C for 8 h to generate TiO_2-terminated surfaces.[34,35] Tapping mode atomic force microscopy (AFM) images and line scans reveal a well-defined terrace-step structure with very flat terraces across several micrometers of the surface, and a minimum step height of 0.4 nm, indicating a single termination. There is no indication of a change in termination from TiO_2 to SrO as a result of the longer oxygen anneal (8 h vs 1 h in Ref. 35), as was seen after annealing for several tens of hours at 1300 °C.[36,37] However, the longer anneal time did result in a more uniformly smooth surface over tens of square micrometers than the shorter 1 h anneals. The substrates were then ultrasonically cleaned in acetone and isopropanol for 5 min each prior to insertion into the vacuum chamber.

Stationary LAO (001) single crystals ($10 \times 10 \times 1$ mm^3) from Crystec (Germany) were used as ablation targets, and the unpolished backsides of the crystals were irradiated to minimize reflection. The geometry of the PLD system has been described elsewhere.[38,39] The vertical distance between the LAO target and the STO substrate was ∼69 mm. A repetition rate of 2 Hz was used for the KrF laser ($\lambda =$ 248 nm), and the laser energy measured prior to transmission through the entrance window was ∼300 mJ with a spot area of nominally 1×10 mm^2 on the target surface after entry. The substrates were rotated during deposition to ensure uniform film composition and thickness. The substrate temperature was ∼700 °C and the O_2 partial pressure in the chamber was maintained at 10 mTorr during deposition. Substrates were cooled to room temperature in 10 mTorr O_2 following growth, and no postgrowth annealing was done. The combination of an off-axis geometry and a relatively high oxygen pressure reduce the likelihood of molten droplet incorporation within films, as well as reducing the ion energy at the growth front. These design features and operating conditions have been shown to result in oxide films with excellent structural quality.[40–42] Surface morphologies for the various films were measured *ex-situ* by tapping-mode AFM using a Digital Instruments Nanoscope III (USA).

Film composition and surface structure were determined by high-energy-resolution x-ray photoelectron spectroscopy (XPS) and reflection high-energy electron diffraction (RHEED), respectively. XPS measurements were carried out using a Scienta SES 200 electron-energy analyzer with a monochromatic Al$K\alpha$ x-ray source, and RHEED patterns were obtained with a Staib electron gun operating at 15 keV. All film surfaces were cleaned using a UV-Ozone treatment on the bench, followed by oxygen plasma cleaning in a preparation chamber appended to the XPS and RHEED chambers prior to measurement. This practice removed all detectable adventitious carbon. Film thicknesses were measured by x-ray reflectivity (XRR) and ellipsometry, and the results are listed in Table I. Film composition and thickness were also measured by Rutherford backscattering spectrometry (RBS) using 2.04-MeV He ions. These measurements were performed using two scattering geometries. In the first geometry, the incident beam was 60° off the surface normal and the scattering angle was 150°. This geometry produced superior mass resolution because of the high scattering angle, and because the backscattered beam traversed close to the surface normal, resulting in a relatively short path length and thus minimal broadening by inelastic scattering. In the other geometry, the incident beam was 7° off the surface normal and the scattering angle was 98°. This geometry produced slightly better depth resolution and higher sensitivity to the weak Al backscattering. RBS spectra were simulated using SIMNRA software.[43]

Lattice parameters and crystal quality were determined using high-resolution x-ray diffraction (HRXRD) with a Philips X'Pert diffractometer equipped with a fixed Cu anode operating at 45 kV and 40 mA. A hybrid monochromator, consisting of four-bounce double-crystal Ge (220) and a Cu x-ray mirror, was placed in the incident beam path to generate

TABLE I. Structural parameters for LAO epitaxial films on STO(001) with various La:Al atom ratios (x).

x	Thickness (Å)	FWHM for (001) RC (deg)	FWHM for (123) RC (deg)	c parameter (Å)	a parameter (Å)	σ_{XRD} (Å)
0.91	153	0.007	0.018	3.748	3.905	0.5
1.01	196	0.015	0.024	3.765	3.905	2
1.11	121	0.021	0.023	3.782	3.905	5
1.22	113	0.031	0.037	3.803	3.870	8

monochromatic Cu$K\alpha$ x rays ($\lambda = 1.540\,56$ Å) with a beam divergence of 12 arc sec. Crystal quality was determined by means of triple-axis rocking curve measurements in which an additional three-bounce Ge (220) channel-cut analyzer was placed in front of a proportional counter to obtain the same divergence as the incident beam. As a result, the diffractometer exhibited an angular precision and reproducibility of 0.0001° and 0.0003°, respectively.

Near-surface composition and the extent of surface hydroxylation were determined by angle-resolved x-ray photoelectron spectroscopy (ARXPS) using the same XPS system described above. The interface composition was determined by dual-beam time-of-flight secondary-ion-mass spectroscopy (TOF-SIMS) depth profiling, using a ToF.SIMS5 instrument from IONTOF GmbH (Germany). To achieve reasonable sputtering rates and maintain a relatively smooth surface in the analysis region, a low-energy (1 keV), high-current (~100 nA), oxygen (O_2^+) beam was used for sputtering and was scanned over an area of 300×300 μm^2. Positive ion signals were collected in a SIMS analysis. To avoid any signal saturation, a pulsed 25-keV Bi_5^+ beam with a current of ~0.05 pA (at 10 kHz pulse rate) was used for the analysis. The Bi_5^+ beam was focused at the center of the O_2^+ sputter crater and scanned over an area of 100×100 μm^2.

III. RESULTS AND DISCUSSION

A. Composition

In our PLD system, the on-axis geometry in which the substrate center is on the plume axis consistently results in La-rich films whereas stoichiometric films result only from an off-axis configuration.[38,39] In order to determine composition by XPS, LAO(001) single crystals were used as standards. We use the La $4d$/Al $2p$ peak area ratio averaged over three as-received single crystals at an emission angle of 90° as being appropriate for stoichiometric LAO films. Figure 1 shows La $4d$ and Al $2p$ spectra for four LAO films. Calibrated against the LAO single crystals, the La/Al atom ratios (x) for these four films are 0.9, 1.0, 1.1, and 1.3, where the uncertainty for all measurements is ±0.1. The magnitude of this experimental uncertainty stems primarily from the uncertainty surrounding the surface termination of bulk LAO(001). In light of the probe depth of XPS measured with Al$K\alpha$ x rays at normal emission at the kinetic energies of the La $4d$ and Al $2p$ peaks (~1.5 nm), a change in surface termination from LaO to AlO_2 is expected to result in an ~20% change in the La $4d$/Al $2p$ peak area ratio based on a simple inelastic attenuation calculation. We thus assign an uncertainty of ±10% to x when based on the La $4d$/Al $2p$ peak area ratio. In the inset of Fig. 1 we compare the La $4d$ and Al $2p$ spectra for stoichiometric film ($x = 1.0$) and bulk LAO(001), where we can see that the curves (and integrated areas) are nearly identical. Also in Fig. 1 are AFM micrographs showing the well-defined step-terrace structure is seen for the surfaces of films for which x is 0.9, 1.0, and 1.1. Very similar La:Al ratios were obtained from RBS, where the La : Al ratios were found to be 0.91(6), 1.01(6), 1.11(6), and 1.22(6) for the same four films. The RBS measurements will be discussed in Sec. III D. We use the RBS atom ratios throughout what follows owing to their smaller experimental uncertainties.

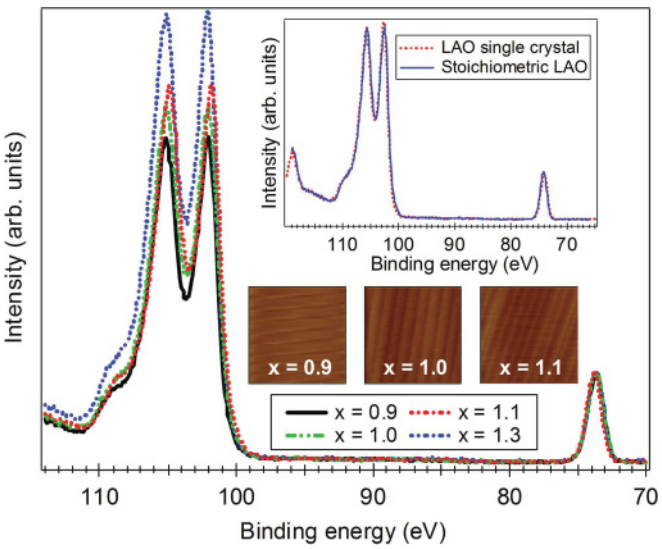

FIG. 1. (Color online) La $4d$ and Al $2p$ XPS spectra for LAO films with La:Al atom ratios (x) of 0.9(1), 1.0(1), 1.1(1) and 1.3(1). Upper inset: Normalized spectra for the stoichiometric film and bulk LAO(001). Lower inset: Tapping mode AFM images for the three well-ordered LAO films.

B. Structure

We show in Fig. 2(a) XRD 2θ-θ scans for the four LAO films. All four exhibit the expected (001)-oriented perovskite structure with no evidence for secondary phase formation. In contrast, phase segregation has been observed in nonstoichiometric STO.[19] If present in sufficient quantities, Sr is incorporated into Sr-rich STO by the formation of $Sr_{m+1}Ti_mO_{3m+2}$ Ruddlesden-Popper (RP) planar phases, and Ti-rich STO exhibits a defective perovskitelike phase of composition $SrTi_2O_5$.[19] However, because the LaO^+ and AlO_2^- planes are charged, an alternating LaO^+-AlO_2^- arrangement is required to minimize the electrostatic energy. Therefore, RP-like phases are not expected to form in LAO.

All four films are fully epitaxial. We show in Fig. 2(b) the {110} φ scan for the stoichiometric LAO film. The overlap of the Bragg peaks for the film and the substrate reveal the expected cube-on-cube structure with the epitaxial relationship LAO (100) [001] ∥ STO (100) [001]. The φ scans for the other three films are the same.

Out-of-plane (002) and in-plane (123) triple-axis rocking curve (RC) measurements were performed to examine epitaxial film quality, as shown in Figs. 2(c) and 2(d). The corresponding full width at half maximum (FWHM) values, after correction for Scherrer contribution, are listed in Table I. The widths of these peaks reflect the extent of mosaic spread in the film and lattice constant spread owing to, for example, degraded structural quality or compositional variation. Generally, all films exhibit reasonably narrow RC widths for both in-plane and out-of-plane scans, revealing good film crystallinity. For comparison, we also measured the RC widths for the (002) and (123) reflections in LAO(001) and STO(001) single crystals, and the FWHM values are 0.030° and 0.016° for LAO, and 0.0076° and 0.0112° for

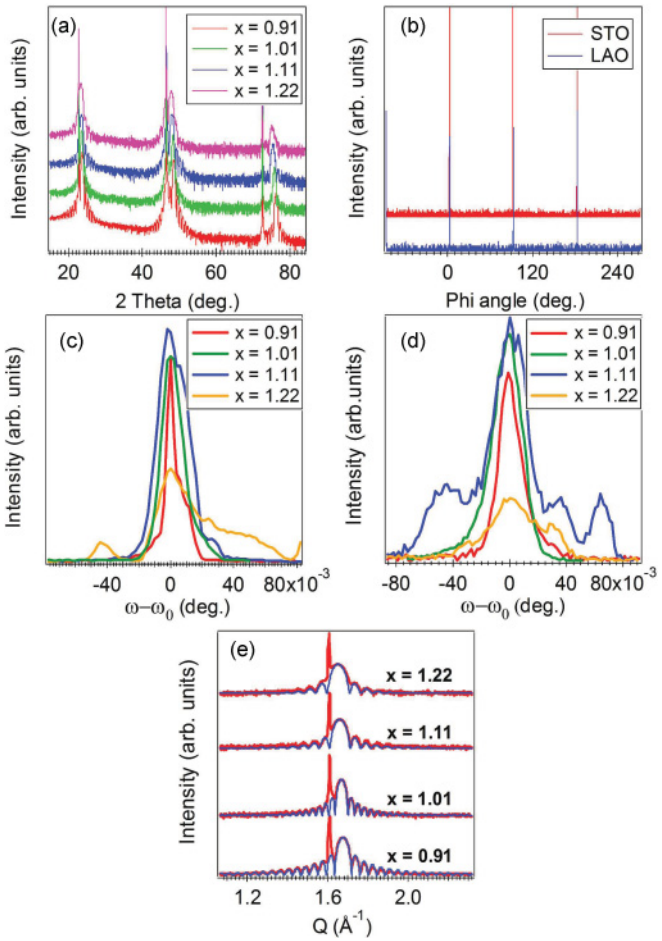

FIG. 2. (Color online) (a) High-resolution 2θ-θ XRD scans for four LAO films. (b) In-plane $\{110\}$ φ scans for the stoichiometric LAO film and its STO substrate. (c) and (d) (002) out-of-plane and (123) in-plane triple-axis RCs, respectively. (e) Finite thickness interference fringes for the various LAO films.

STO, respectively. These RC widths are not as low as those measured for bulk single crystals of other materials with higher structural quality. The rather large FWHM values for the LAO single crystal are owing to its mosaic spread and twinned structure, which may not be present in the epitaxial films. The similarity between the FWHM values of the STO substrates and those of the films (Table I) reveal that the structural quality of the films is limited by the structural quality of the substrates.

Good crystallographic film quality is further confirmed by the presence of finite thickness interferences or Kiessig fringes on the LAO (001) Bragg reflections for the different films,[44,45] as shown in Fig. 2(e). The presence and persistence of these fringes are a measure of the crystalline order of atomic planes perpendicular to the growth direction, as well as the flatness of the surface and the interface. To quantify overall film quality from these fringes, the data were fit to a model that takes into account the interference of wave fields scattered by atomic planes over the finite thickness of the film. The resulting expression is

$$I(Q) = \frac{\sin^2(QL/2)}{\sin^2(Qd/2)} \exp(-|Q - 2\pi/d|\sigma_{\mathrm{XRD}}). \qquad (1)$$

Here, $I(Q)$ is the scattered x-ray intensity, Q is the scattering vector given by $Q = (4\pi/\lambda)\sin\theta$, where λ is the x-ray wavelength and θ is the angle of x-ray incidence with respect to the surface, L is the film thickness, d is the layer spacing along (001), and σ_{XRD} is the overall measure of film crystallinity and surface and interface roughness.[44,45] The values of σ_{XRD} extracted from the fits are listed in Table I for the film set. Ironically, the La-deficient film ($x = 0.91$) exhibits a lower value of σ_{XRD} than the stoichiometric film. However, σ_{XRD} rapidly increases as the films become more La rich, revealing a significant degradation in overall epifilm quality.

The out-of-plane lattice parameter (c) for the LAO films and their respective STO substrate were determined for the original film set plus one additional 82-Å film for which $x = 0.86$. The c lattice parameter was obtained by averaging the values obtained from the positions of the ($00l$) Bragg reflections, where $l = 1$, 2, and 3. The resulting values of c are 3.728, 3.748, 3.765, 3.782, and 3.803 Å for $x = 0.86$, 0.91, 1.01, 1.10, and 1.22, respectively, and $c = 3.905$ for STO(001). All c values (except that for $x = 1.22$) are smaller than the value for LAO(001) (3.791 Å), indicating compression along c owing to the in-plane tensile stress exerted by the substrate. The in-plane lattice parameters (a and b) for the film set and the substrate were determined from (hkl) Bragg reflections for which h, k, $l \neq 0$, primarily at 2θ values larger than 80°, in order to minimize errors. We averaged interplanar spacing values for the (113), (123), and (114) reflections for each specimen. The resultant values are $a = b = 3.905$ Å for $x = 0.86$, 0.91, 1.01, and 1.10, revealing in-plane coherence with the substrate. In contrast, $a = b = 3.870$ Å for $x = 1.22$. These results indicate that, for $x \leqslant 1.10$, the critical thickness (h_c) exceeds the film thickness, as listed in Table I. Critical thicknesses in excess of 100 Å are not expected for a system in which the lattice mismatch is so large (−2.91%). Within the framework of elastic theory, the h_c value of a system of two oxides in intimate contact can be calculated by either the Matthews-Blakeslee (MB, mechanical equilibrium) or People-Bean (PB, energy equilibrium) models,[46–49]

$$h_c^{\mathrm{MB}} = \frac{b}{8\pi f}\frac{(1 - \nu\cos^2\theta)}{(1+\nu)\cos\lambda}\ln\left(\frac{\beta h_c}{b}\right), \qquad (2)$$

$$h_c^{\mathrm{PB}} = \left(\frac{b}{f}\right)\left[\frac{1}{4\pi(1+\nu)}\right]\left[\ln\left(\frac{h_c}{b}\right) + 1\right], \qquad (3)$$

where b is the magnitude of the Burgers vector for dislocations, ν is the average Poisson ratio for the film material,[50] f is the misfit strain between film and substrate, θ is the angle between dislocation line and the Burgers vector, λ is the angle between the slip direction and the direction perpendicular to the line of intersection of the slip plane and the interface, and β is the cutoff radius of the dislocation and is estimated to be ∼4.[51] The resulting values for h_c for LAO/STO(001) are 17 and 23 Å for the MB and PB models, respectively. Both are considerably smaller than the experimental values, which exceed 100 Å for all films except for $x = 1.22$, which is partially relaxed. Both MB and PB models assume an abrupt interface that results in localization of the strain directly at the interface. However, if intermixing occurs, the strain would be distributed over a larger distance, resulting in a larger value of h_c. Intermixing is discussed in more detail below. All films exhibit values of a

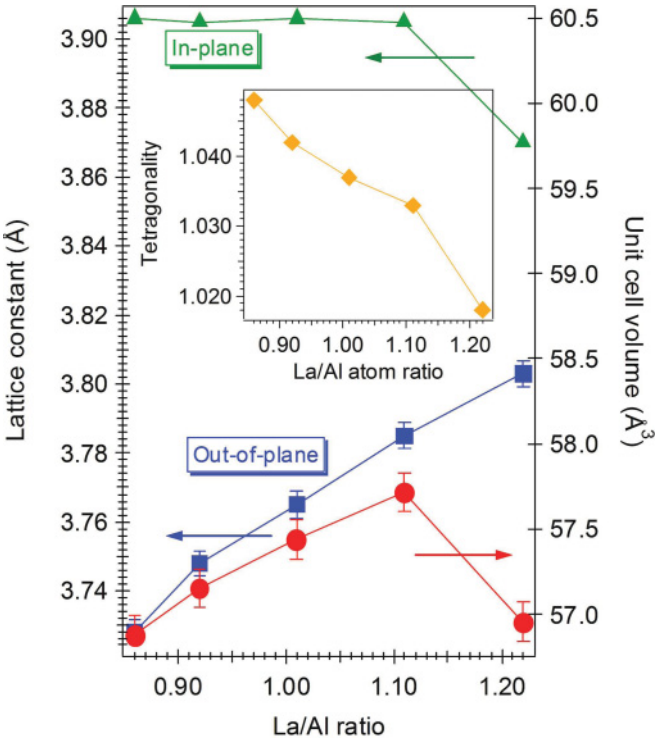

FIG. 3. (Color online) Dependence of lattice parameter and unit-cell volume as well as tetragonality (inset) on La : Al atom ratio from XRD data.

and b that exceed c, as expected for in-plane tensile stress. The tetragonality (a/c) is 1.048, 1.042, 1.037, 1.033, and 1.018 for $x = 0.86$, 0.91, 1.01, 1.10, and 1.22, respectively. RBS RC measurements performed on a few samples (not shown) yielded the same tetragonality value, as did XRD.

Interestingly, an experimental critical thickness has been reported also for LAO/STO(001) grown by MBE.[52] This value ($h_c = 38$ Å) is considerably lower than what we have measured. However, these authors did not measure either the film composition or the extent of intermixing at the interface, both of which are expected to influence h_c.

The dependences of the in-plane and out-of-plane lattice parameters as well as the unit-cell volume and tetragonality on the La : Al atom ratio (x) are shown in Fig. 3. All films except those for which $x = 1.22$ are coherently strained to the substrate, and the $x = 1.22$ specimen is partially relaxed. There is a significant increase in c and a corresponding decrease in tetragonality with increasing La : Al ratio. The decrease in tetragonality with x indicates a reduction in strain energy within the film with increasing La. The unit-cell volume increases with x for all values except $x = 1.22$. The expansion of c and the unit-cell volume increase from $x = 0.86$ to 1.10 could be ascribed to the incorporation of excess La ions into the lattice. The ionic radii of six-fold coordinate Al^{3+} and 12-fold coordinate La^{3+} are 0.53 and 1.36 Å, respectively.[53] The much larger size of La^{3+} suggests that excess La in the lattice would introduce significant amounts of disorder. For $x > 1.0$, three kinds of defects could form, depending on the *absolute* concentrations of La and Al within the film: (i) Al vacancies, which could occur if the film is stoichiometric in La but deficient in Al, (ii) La at Al sites (La_{Al}), which could occur if the film is deficient in Al but has excess La, or (iii) La interstitials (La_i), which could occur if the film is stoichiometric in Al but has excess La. RBS RC measurements would be sensitive to La_i if present in sufficient quantities; La_i would appear as a peak along the channeling direction if these species occur in well-defined positions in the lattice. However, RC measurements on the films for which $x > 1.0$ do not show a peak along the channeling direction. Moreover, La_{Al} antisite defects are energetically unfavorable owing to the La^{3+}-Al^{3+} size mismatch and can thus be ruled out. Therefore, Al vacancy formation seems to be the most likely scenario for $x > 1.0$.

RBS RCs for the $x < 1.0$ film cannot detect interstitial Al (Al_i) owing to its lack of sensitivity to Al. However, if there is any Al_i in the $x < 1.0$ film, the unit-cell volume should be larger than that of the stoichiometric film. However, this is not the case, suggesting that La vacancies and/or Al_{La} antisites may be occurring in the $x < 1.0$ film. Note that the ionic radii of La and Sr (or Al and Ti) are quite similar.[53] Therefore, even considering possible cation intermixing at the interface (details are found in Sec. III D), the above discussion is still valid.

C. The nature of the surface

We show RHEED patterns for the film set in Fig. 4. For the $x = 0.91$ and 1.01 films, the diffraction rods are sharp and streaky patterns are seen in both high-symmetry azimuths, indicating that the film surfaces are well ordered and flat, consistent with the AFM results. In contrast, the $x = 1.11$ and 1.22 films exhibit weaker streaks (higher background), indicative of lower structural quality and higher disorder, consistent with the XRD results.

We show in Figs. 5(a) and 5(b) ARXPS measurements for the La 4d and Al 2p peak areas in the (010) azimuth plane for the film set and for bulk LAO (001). Here, the polar angle $\theta = 90^\circ$ is defined as the surface normal direction. The epitaxial films and the bulk crystal exhibit nearly the same diffraction modulation as expected for epitaxial films. The strong La 4d peaks at $\theta = 45^\circ$ and 90° are the so-called "forward-focusing" peaks associated with elastic scattering along the [101] and [001] low-index direction in the

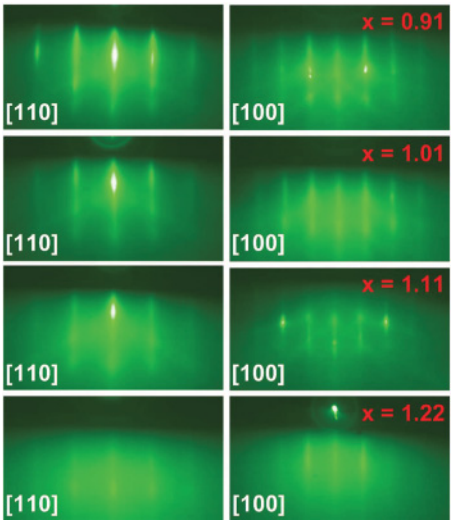

FIG. 4. (Color online) RHEED patterns along [110] and [100] azimuths for the various LAO films.

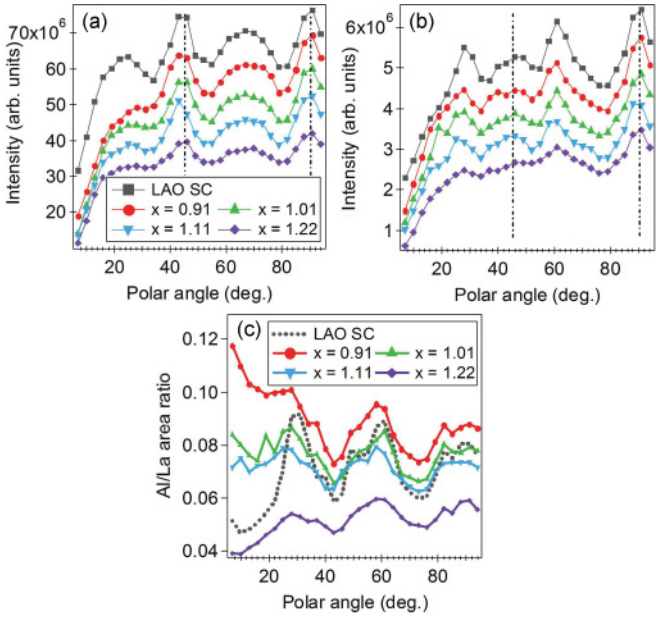

FIG. 5. (Color online) (a) La 4*d* and (b) Al 2*p* XPS polar scans in the (010) azimuth, along with (c) the Al 2*p*/La 4*d* peak area ratio for the various LAO films and bulk LAO(001).

perovskite structure. Forward focusing universally occurs for high-kinetic-energy photoelectrons propagating along a close-packed, low-index direction.[54,55] The fact that the [101] forward-focusing peak falls at a slightly lower takeoff angle for the films than for the bulk crystal reveals tetragonal distortion in the films, consistent with XRD and RBS. The diminution in the diffraction modulation for the $x = 1.22$ film reveals increased structural disorder relative to the other films. Figure 5(c) shows the dependence of the Al 2*p*/La 4*d* peak area ratio on the takeoff angle for the four films and the bulk crystal. This ratio increases with decreasing takeoff angle for the $x = 0.91$ film, suggesting an Al enhancement in the near-surface region of this film. This ratio does not increase at lower, more surface-sensitive angles for $x = 1.01$ and 1.10, and actually drops for $x = 1.22$, consistent with Al depletion of the surface for the latter.

All four film surfaces are hydroxylated, but the extent of hydroxylation is greater for the La-rich film, as seen in Figs. 6(a)–6(d). Here we show the O 1*s* core-level XPS spectra as a function of takeoff angle. Each spectrum consists of the lattice O peak at ~531 eV and the weaker OH feature at ~533 eV.[56] Figure 6(e) shows the integrated peak areas for these two features versus the angle for the $x = 1.01$ film. The lattice peak intensity (I_{LAO}) increases with increasing takeoff angle, in keeping with the instrument response function. In contrast, the OH intensity (I_{OH}) increases at low angles, as expected for a surface-bound species. This observation was made for all four films, but the amount of surface OH was found to increase with increasing *x*. To illustrate, we plot in Fig. 6(f) the peak area ratio I_{OH}/I_{LAO} versus the angle for the $x = 0.91$ and 1.22 films, along with the RHEED patterns, which show the increased surface disorder at higher *x*. There is a clear increase in surface hydroxylation with increasing La concentration in the film and the attendant extent of surface disorder.[57] Hydroxylation also represents a means by which

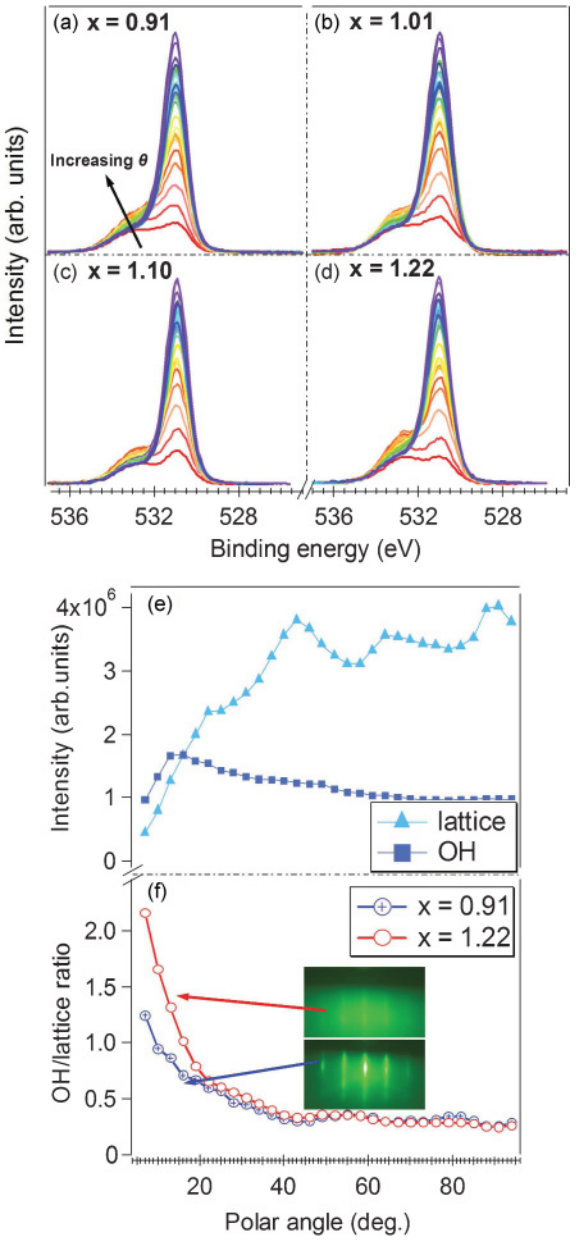

FIG. 6. (Color online) O 1*s* XPS spectra vs takeoff angle for the different LAO films (a)–(d). (e) OH and lattice O 1*s* peak areas vs take-off angle for the stoichiometric film, (f) along with OH/lattice peak area ratio vs takeoff angle for the $x = 0.91$ and 1.22 films (f).

the surface dipole resulting from the polar nature of LAO may be eliminated.

D. Interfacial intermixing

Cation intermixing at the interface is revealed by RBS and SIMS measurements. Figure 7(a) shows RBS away from any channeling directions at a scattering angle of 98°, along with simulations for the stoichiometric LAO film. We have modeled both abrupt and optimized intermixing configurations. As seen in the middle of Fig. 7(b), the abrupt-interface model predicts that the valley between the La and Sr peaks should go to zero counts. However, counts are clearly present here and these counts cannot be accounted for without modeling La

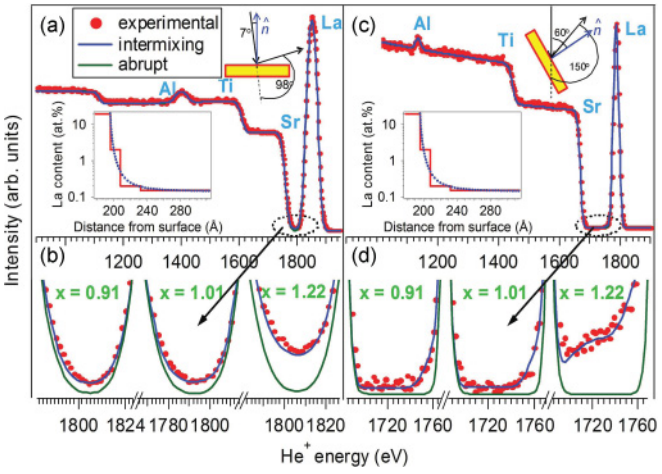

FIG. 7. (Color online) Random RBS spectrum (filled red circles) and simulations based on abrupt (solid green curves) and intermixing (solid blue curves) model for stoichiometric and nonstoichiometric LAO films. The spectra in (a) and (b) were collected at a scattering angle of 98°, while those in (c) and (d) were collected at 150°.

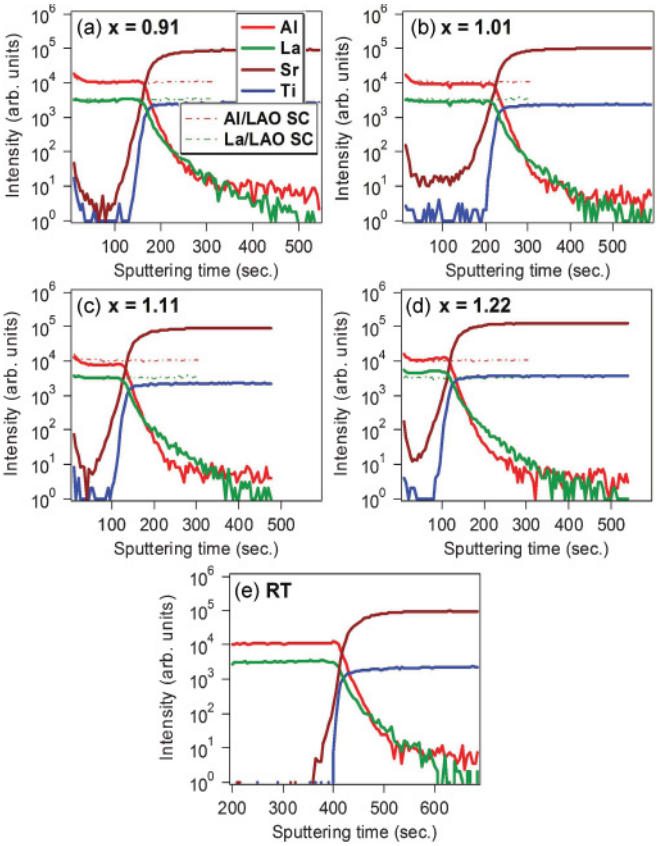

FIG. 8. (Color online) TOF-SIMS depth profiles for the four crystalline LAO films, an amorphous LAO film grown at RT, and a LAO(001) single crystal.

diffusion into the STO substrate. The La atom profile that gives the best agreement with experiment includes three distinct La-containing regions within the STO substrate [see inset of Fig. 7(a)]: (i) 2.0 at. % La from a depth of 196 to 208 Å, (ii) 0.2 at. % La from 208 to 232 Å, and (iii) 0.15 at. % La from 232 to 328 Å. The first of these regions corresponds to the intermixed region in the vicinity of the interface noted elsewhere.[7,11,12,28] The second and third regions correspond to a deep diffusion tail that has not been previously observed. Likewise, the model includes a Sr diffusion profile within the LAO film with 0.35 at. % Sr in the top 147 Å, 0.55 at. % Sr from 147 to 172 Å, and 1.00 at. % Sr from 172 to 196 Å. La-Sr intermixing also occurs in the three nonstoichiometric LAO films, as shown in Fig. 7(b). Here we compare the valley region between the La and Sr peaks to abrupt and optimized intermixed simulations and again find much better agreement when intermixing is modeled. The atom profiles extracted from the intermixed simulations for nonstoichiometric films are similar to those obtained from the stoichiometric film [Fig. 7(b)]. The extent of intermixing appears to be most extensive for the most La-rich film ($x = 1.22$). La-Sr intermixing is further revealed by RBS spectra taken from the higher scattering angle of 150° for which we have better mass resolution [Figs. 7(c) and 7(d)]. Again, the abrupt models cannot account for the presence of counts in the valley, whereas the optimized intermixed models are able to capture these counts. While these atom profiles do not represent unique solutions to the RBS data, they do point to the undeniable presence of La (Sr) in the STO (LAO) and are at least of qualitative value, as revealed by the insets in Figs. 7(a) and 7(c). RBS is very sensitive to La and somewhat sensitive to Sr because the backscattering cross section goes as Z^2, allowing us to track at least La at concentrations of <1 at. %. However, RBS is not as sensitive to Ti and Al owing to their lower Z values. Therefore, we turn to TOF-SIMS depth profiling to probe their diffusion profiles.

Figures 8(a)–8(d) show TOF-SIMS sputter depth profiles for all four LAO films as well as a LAO(001) single-crystal standard. The La : Al atom ratios obtained by comparing the SIMS ratios for the films to those of the bulk crystal are in qualitative agreement with the values obtained from XPS and RBS. In order to extract atom diffusion profiles, it is essential to determine background levels for an "abrupt" sample. This is best done by growing a film on STO(001) at room temperature (RT) in order to kinetically limit intermixing, and then using the near surface region to establish background counts for Sr and Ti, and the substrate after sputtering away all the film to establish background values for La and Al. Depth profiles for a 400-Å-thick LAO film on STO(001) grown at RT are shown in Fig. 8(e). The Sr and Ti signals near the surface are essentially 0 cps, whereas the La and Al signals after ~600 s of sputtering are ~1–2 and ~5–10 cps, respectively. These values establish our background signals for the four elements. Returning to Figs. 8(a)–8(d), it is clear that for all four films that the Sr signal persists at levels above background in the near-surface region, albeit at levels that are factors of 10^3–10^4 below the signals measured after sputtering deep into the substrate. In contrast, the Ti signal goes to values very near background at the surface. The La and Al signals decay slowly as we sputter into the substrate, eventually reaching background levels after a few hundred seconds of sputtering. This behavior can result from either indiffusion or knock-on, or a combination thereof, as discussed below.

In order to compare the behaviors of each element in the four films, we replot the data in Figs. 8(a)–8(e) on a per

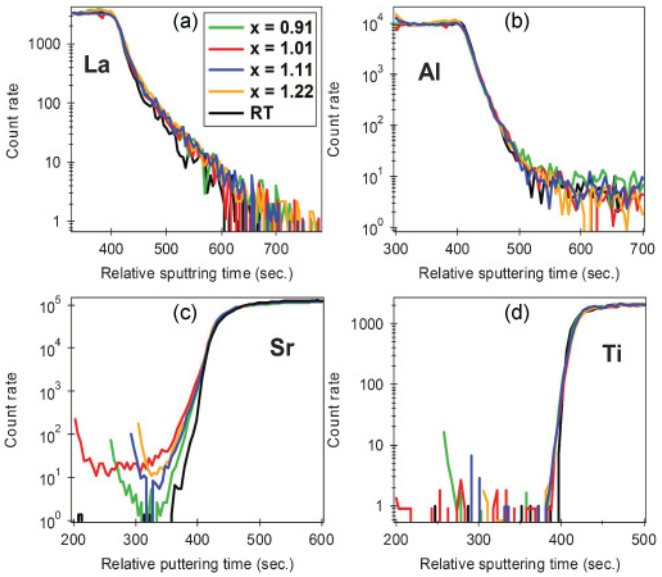

FIG. 9. (Color online) La, Al, Sr, and Ti depth profiles for the various films after shifting to common transition points along the time axes, and normalizing to common count rates in the pure phases for easy comparison.

element basis, and the results are shown in Figs. 9(a)–9(d). To make a direct comparison, the onset of change has been shifted to common values of sputter time with respect to the interface, and the "bulk" signals have been normalized to a set of common values. It is clear that Sr, but not Ti, diffuses out to the surface at trace concentrations. For all four crystalline films, the Sr and Ti signals reach ∼1% of their bulk STO values at sputter times of ∼370 and ∼385 s, respectively, which correspond to distances of ∼3 and ∼1.5 nm out from the interface. Additionally, a Sr signal is measured on the LAO side of the interface for the film grown at RT; the Sr signal drops to ∼0.5% of the bulk value after a sputter time of ∼385 s, which corresponded to a distance of ∼1.5 nm out from the interface. Likewise, for all crystalline films, the La signal does not drop to 1% of the bulk value until ∼500 s of sputtering, corresponding to a distance of ∼10 nm below the interface. Moreover, the Al signal does not drop to 1% of the bulk value until ∼470 s (∼7 nm below the interface). The persistence of these signals may be due to knock-on effects rather than, or in addition to, La and Al indiffusion. The La signal associated with the $x = 1.22$ film persists deeper into the substrate than that of the other crystalline films, and the La signal for the RT film falls off faster than those of the crystalline films grown at elevated temperature. These results suggest that at least some of the La signal within the substrates is due to indiffusion, as also revealed by RBS. Although the La and Al signals within the substrate may be at least partially owing to knock-on effects induced by the Bi_5^+ analysis beam during profiling, the presence of Sr and Ti signals in the film well away from the interface cannot be accounted for by anything other than outdiffusion. Intermixing at the interface of stoichiometric LAO films on STO(001) grown under the same conditions was corroborated by angle-resolved XPS.[38]

Based on our first-principles calculations, intermixing appears to be unavoidable because of thermodynamic instability at the abrupt LAO/STO interface, and the role that cation intermixing plays in eliminating interfacial dipoles.[33] However, there are three other potential causes that must be considered: (1) kinetically driven interdiffusion, (2) energetic implantation and host cation displacement caused by ions in the ablation plume, and (3) Sr vacancy formation in the near-surface region of STO. The first is probably not significant because our study of PLD-grown LAO/STO interfaces prepared by others did not reveal enhanced interdiffusion in specimens subjected to postgrowth annealing as compared to as-grown heterojunctions.[33] Addressing the second possibility, Tyrrell *et al.*[58–60] have investigated laser-target interaction dynamics and measured the kinetic-energy distribution of different species within the plume for many solid materials. These authors found that most ionic species in the plume exhibit kinetic energies from several to a few tens of eV. These energies are significantly higher than the typical thermal energy found in atom beams generated by an effusion cell, ∼0.1 eV. Although we used an off-axis PLD geometry with a large working distance and high oxygen pressure to minimize ion energies in the plume, effect (2) cannot be completely eliminated. Additionally, it has been demonstrated that annealing TiO_2-terminated STO at 600 °C in an oxygen ambient results in Sr vacancy creation.[12,61,62] If a similar effect occurs when growing LAO on STO, La indiffusion may be promoted because of the similar ionic radii for La^{3+} and Sr^{2+}.[53] Therefore, although intermixing is predicated to be thermodynamically favored, the combination of energetic ions and the subsurface substrate may also promote intermixing. In support of this conclusion, Jalan *et al.*[63] found that La diffusion from high-quality MBE-grown La-doped STO into the adjacent buffer layers did not occur at comparable temperatures to those used here.

IV. CONCLUSION

High-quality epitaxial LAO films both on and off stoichiometry were deposited on TiO_2-terminated STO (001) substrates by off-axis PLD, and the resulting structures and compositions were characterized by using several techniques. Both crystalline quality and tetragonality decrease with increasing La/Al cation ratio. The critical thickness for all compositions is significantly larger than predicted by elastic theory in which an abrupt interface is assumed. Higher than expected critical thicknesses are consistent with interfacial intermixing, which would grade the strain over a few to several nanometers. Rather extensive cation intermixing is observed for all compositions, and these results show the inherent instability of the LAO/STO interface. This description of the system is at odds with the idealized abrupt interface model commonly assumed in the LAO/STO literature.

ACKNOWLEDGEMENTS

This work was supported by the Office of Science, Division of Materials Sciences and Engineering, US Department of Energy, and was performed in the Environmental Molecular Sciences Laboratory, a national scientific user facility sponsored by the Office of Biological and Environmental Research of the Department of Energy and located at Pacific Northwest National Laboratory.

*sa.chambers@pnl.gov

[1] J. Wang, J. B. Neaton, H. Zheng, V. Nagarajan, S. B. Ogale, B. Liu, D. Viehland, V. Vaithyanathan, D. G. Schlom, U. V. Waghmare, N. A. Spaldin, K. M. Rabe, M. Wuttig, and R. Ramesh, Science **299**, 1719 (2003).

[2] M. Huijben, A. Brinkman, G. Koster, G. Rijnders, H. Hilgenkamp, and D. H. A. Blank, Adv. Mater. **21**, 1665 (2009).

[3] A. Ohtomo and H. Y. Hwang, Nature (London) **427**, 423 (2004).

[4] S. Thiel, G. Hammerl, A. Schmehl, C. W. Schneider, and J. Mannhart, Science **313**, 1942 (2006).

[5] M. Huijben, G. Rijnders, D. H. A. Blank, S. Bals, S. Van Aert, J. Verbeeck, G. Van Tendeloo, A. Brinkman, and H. Hilgenkamp, Nat. Mater. **5**, 556 (2006).

[6] N. Reyren, S. Thiel, A. D. Caviglia, L. F. Kourkoutis, G. Hammerl, C. Richter, C. W. Schneider, T.Kopp, A.-S. Ruetschi, D. Jaccard, M. Gabay, D. A. Muller, J.-M. Triscone, and J. Mannhart, Science **317**, 1196 (2007).

[7] N. Nakagawa, H. Y. Hwang, and D. A. Muller, Nat. Mater. **5**, 204 (2006).

[8] M. Salluzzo, J. C. Cezar, N. B. Brookes, V. Bisogni, G. M. DeLuca, C. Richter, S. Thiel, J. Mannhart, M. Huijben, A. Brinkman, G. Rijnders, and G. Ghiringhelli, Phys. Rev. Lett. **102**, 166804 (2009).

[9] G. Herranz, M. Basletic, M. Bibes, C. Carretero, E. Tafra, E. Jacquet, K. Bouzehouane, C. Deranlot, A. Hamzic, J. M. Broto, A. Barthelemy, and A. Fert, Phys. Rev. Lett. **98**, 216803 (2007).

[10] W. Siemons, G. Koster, H. Yamamoto, W. A. Harrison, G. Lucovsky, T. H. Geballe, D. H. A. Blank, and M. R. Beasley, Phys. Rev. Lett. **98**, 196802 (2007).

[11] P. R. Willmott, S. A. Pauli, R. Herger, C. M. Schleputz, D. Martoccia, B. D. Patterson, B. Delley, R. Clarke, D. Kumah, C. Cionca, and Y. Yacoby, Phys. Rev. Lett. **99**, 155502 (2007).

[12] A. S. Kalabukhov, Y. A. Boikov, I. T. Serenkov, V. I. Sakharov, V. N. Popok, R. Gunnarsson, J. Borjesson, N. Ljustina, E. Olsson, D. Winkler, and T. Claeson, Phys. Rev. Lett. **103**, 146101 (2009).

[13] S. A. Chambers, Adv. Mater. (Weinheim, Ger.) **22**, 219 (2010).

[14] J. L. Maurice, C. Carretero, M. J. Casanove, K. Bouzehouane, S. Guyard, E. Larquet, and J. P. Contour, Phys. Status Solidi A **203**, 2209 (2006).

[15] T. Ohnishi, M. Lippmaa, T. Yamamoto, S. Meguro, and H. Koinuma, Appl. Phys. Lett. **87**, 241919 (2005).

[16] T. Ohnishi, K. Shibuya, T. Yamamoto, and M. Lippmaa, J. Appl. Phys. **103**, 103703 (2008).

[17] T. Ohnishi, H. Koinuma, and M. Lippmaa, Appl. Surf. Sci. **252**, 2466 (2006).

[18] B. Jalan, P. Moetakef, and S. Stemmer, Appl. Phys. Lett. **95**, 032906 (2009).

[19] P. Fisher, H. Du, M. Skowronski, P. A. Salvador, O. Maksimov, and X. Weng, J. Appl. Phys. **103**, 013519 (2008).

[20] D. Fuchs, M. Adam, P. Schweiss, S. Gerhold, S. Schuppler, R. Schneider, and B. Obst, J. Appl. Phys. **88**, 1844 (2000).

[21] H. W. Jang, A. Kumar, S. Denev, M. D. Biegalski, P. Maksymovych, C. W. Bark, C. T. Nelson, C. M. Folkman, S. H. Baek, N. Balke, C. M. Brooks, D. A. Tenne, D. G. Schlom, L. Q. Chen, X. Q. Pan, S. V. Kalinin, V. Gopalan, and C. B. Eom, Phys. Rev. Lett. **104**, 197601 (2010).

[22] S. Lee, Z. K. Liu, M. H. Kim, and C. A. Randall, J. Appl. Phys. **101**, 054119 (2007).

[23] S. Lee, G. A. Rossetti, Z. K. Liu, and C. A. Randall, J. Appl. Phys. **105**, 093519 (2009).

[24] F. Y. Hsu, C. C. Leu, and C. T. Hu, J. Electrochem. Soc. **157**, G57 (2010).

[25] J. A. Chaos, J. Gonzalo, C. N. Afonso, J. Perriere, and M. T. Garcia-Gonzalez, Appl. Phys. A **72**, 705 (2001).

[26] H. Xia, Y. S. Meng, L. Lu, and G. Ceder, J. Electrochem. Soc. **154**, A737 (2007).

[27] J. Verbeeck, S. Bals, A. N. Kravtsova, D. Lamoen, M. Luysberg, M. Huijben, G. Rijnders, A. Brinkman, H. Hilgenkamp, D. H. A. Blank, and G. Van Tendeloo, Phys. Rev. B **81**, 085113 (2010).

[28] C. L. Jia, S. B. Mi, M. Faley, U. Poppe, J. Schubert, and K. Urban, Phys. Rev. B **79**, 081405(R) (2009).

[29] R. Pentcheva and W. E. Pickett, Phys. Rev. B **74**, 035112 (2006).

[30] Z. S. Popovic, S. Satpathy, and R. M. Martin, Phys. Rev. Lett. **101**, 256801 (2008).

[31] J. Lee and A. A. Demkov, Phys. Rev. B **78**, 193104 (2008).

[32] K. Janicka, J. P. Velev, and E. Y. Tsymbal, Phys. Rev. Lett. **102**, 106803 (2009).

[33] S. A. Chambers, M. H. Engelhard, V. Shutthanandan, Z. Zhu, T. C. Droubay, L. Qiao, P. V. Sushko, T. Feng, H. D. Lee, T. Gustafsson, E. Garfunkel, A. B. Shah, Z. J. M., and Q. M. Ramasse, Surf. Sci. Rep. **65**, 317 (2010).

[34] M. Kawasaki, K. Takahashi, T. Maeda, R. Tsuchiya, M. Shinohara, O. Ishiyama, T. Yonezawa, M. Yoshimoto, and H. Koinuma, Science **266**, 1540 (1994).

[35] G. Koster, B. L. Kropman, G. Rijnders, D. H. A. Blank, and H. Rogalla, Appl. Phys. Lett. **73**, 2920 (1998).

[36] R. Bachelet, F. Sanchez, F. J. Palomares, C. Ocal, and J. Fontcuberta, Appl. Phys. Lett. **95**, 141915 (2009).

[37] H. Wei, L. Beuermann, J. Helmbold, G. Borchardt, V. Kempter, G. Lilienkamp, and W. Maus-Friedrichs, J. Eur. Ceram. Soc. **21**, 1677 (2001).

[38] L. Qiao, T. C. Droubay, V. Shutthanandan, Z. Zhu, P. V. Sushko, and S. A. Chambers, J. Phys. Condens. Matter **22**, 312201 (2010).

[39] T. C. Droubay, L. Qiao, T. C. Kaspar, M. H. Engelhard, V. Shutthanandan, and S. A. Chambers, Appl. Phys. Lett. **97**, 124105 (2010).

[40] T. C. Kaspar, T. Droubay, S. M. Heald, P. Nachimuthu, C. M. Wang, V. Shutthanandan, C. A. Johnson, D. R. Gamelin, and S. A. Chambers, New J. Phys. **10**, 055010 (2008).

[41] A. Ney, K. Ollefs, S. Ye, T. Kammermeier, V. Ney, T. C. Kaspar, S. A. Chambers, F. Wilhelm, and A. Rogalev, Phys. Rev. Lett. **100**, 157201 (2008).

[42] T. C. Droubay, D. J. Keavney, T. C. Kaspar, S. M. Heald, C. M. Wang, C. A. Johnson, K. M. Whitaker, D. R. Gamelin, and S. A. Chambers, Phys. Rev. B **79**, 155203 (2009).

[43] M. Mayer, *SIMNRA User's Guide 6.04* (Max-Planck-Institut für Plasmaphysik, Garching, Germany, 2008).

[44] S. A. Chambers, J. Phys. Condens. Matter **20**, 264004 (2008).

[45] T. C. Kaspar, T. Droubay, V. Shutthanandan, S. M. Heald, C. M. Wang, D. E. McCready, S. Thevuthasan, J. D. Bryan, D. R. Gamelin, A. J. Kellock, M. F. Toney, X. Hong, C. H. Ahn, and S. A. Chambers, Phys. Rev. B **73**, 155327 (2006).

[46] J. W. Matthews and A. E. Blakeslee, J. Cryst. Growth **27**, 118 (1974).

[47] R. People and J. C. Bean, Appl. Phys. Lett. **47**, 322 (1985).

[48] Y. B. Chen, H. P. Sun, M. B. Katz, X. Q. Pan, K. J. Choi, H. W. Jang, and C. B. Eom, Appl. Phys. Lett. **91**, 252906 (2007).

[49]S. Venkatesan, A. Vlooswijk, B. J. Kooi, A. Morelli, G. Palasantzas, J. T. M. De Hosson, and B. Noheda, Phys. Rev. B **78**, 104112 (2008).
[50]X. Luo and B. Wang, J. Appl. Phys. **104**, 073518 (2008).
[51]J. Q. He, R. F. Klie, G. Logvenov, I. Bozovic, and Y. M. Zhu, J. Appl. Phys. **101**, 073906 (2007).
[52]C. Merckling, M. El-Kazzi, G. Delhaye, V. Favre-Nicolin, Y. Robach, M. Gendry, G. Grenet, G. Saint-Girons, and G. Hollinger, J. Cryst. Growth **306**, 47 (2007).
[53]R. D. Shannon and C. T. Prewitt, Acta Crystallogr. B **25**, 925 (1969).
[54]S. A. Chambers, Adv. Phys. **40**, 357 (1991).
[55]S. A. Chambers, Science **248**, 1129 (1990).
[56]S. A. Chambers, Y. Liang, Z. Yu, R. Droopad, and J. Ramdani, J. Vac. Sci. Technol. A **19**, 934 (2001).
[57]A. M. De Asha, J. T. S. Critchley, and R. M. Nix, Surf. Sci. **405**, 201 (1998).
[58]G. C. Tyrrell, L. G. Coccia, T. H. York, and I. W. Boyd, Appl. Surf. Sci. **96**, 227 (1996).
[59]G. C. Tyrrell, T. York, N. Cherief, D. Givord, J. Lawler, J. G. Lunney, M. Buckley, and I. W. Boyd, Microelectron. Eng. **25**, 247 (1994).
[60]G. C. Tyrrell, T. H. York, L. G. Coccia, and I. W. Boyd, Appl. Surf. Sci. **96**, 769 (1996).
[61]R. Meyer, R. Waser, J. Helmbold, and G. Borchardt, Phys. Rev. Lett. **90**, 105901 (2003).
[62]K. Gomann, G. Bochardt, M. Schulz, A. Gomann, W. Maus-Friedrichs, B. Lesage, O. Kaitasov, S. Hoffman-Eifert, and T. Schneller, Phys. Chem. Chem. Phys. **7**, 2053 (2005).
[63]B. Jalan, S. Stemmer, S. Mack, and S. J. Allen, Phys. Rev. B **82**, 081103(R) (2010).